analytical chemistry

Article

Cite This: Anal. Chem. 2018, 90, 6020−6027

pubs.acs.org/ac

In Vivo Two-Photon Fluorescence Imaging of the Activity of the Inflammatory Biomarker LTA_4H in a Mouse Pneumonia Model

Hui Wang,[†] Ke Xue,[†] Ping Li,* Yuyun Yang, Zixu He, Wei Zhang, Wen Zhang, and Bo Tang*

College of Chemistry, Chemical Engineering and Materials Science, Institute of Biomedical Sciences, Collaborative Innovation Center of Functionalized Probes for Chemical Imaging in Universities of Shandong, Key Laboratory of Molecular and Nano Probes, Ministry of Education, Shandong Provincial Key Laboratory of Clean Production of Fine Chemicals, Shandong Normal University, Jinan 250014, People's Republic of China

Supporting Information

ABSTRACT: Severe atmospheric haze caused by industrial pollution has severely affected human health and led to the increasing incidence of cardiopulmonary diseases, including pneumonia. Conventional methods for diagnosis of pneumonia are complicated and tedious, and current clinical imaging techniques might cause organ injuries to some extent. Therefore, an accurate, fast, and intact imaging method must be developed to diagnose pneumonia in the early stages. In this study, we propose a new two-photon fluorescence probe, named as ASPC, for detection of the activity of the inflammatory biomarker LTA_4H through specific recognition and cleavage of amides containing the unnatural amino acid L-AspBzl. The activity of LTA_4H in the lung tissues of mice was rapidly and accurately monitored for the first time and could be an indicator for diagnosis of pneumonia. The severity of pneumonia in mice caused by haze particulate was determined through imaging the activity of LTA_4H as biomarker and confirmed using a commercial ELISA kit of interleukin-1β. This work provides a promising method for clinical detection of pneumonia and for screening specific depressors of LTA_4H as potential drug candidates.

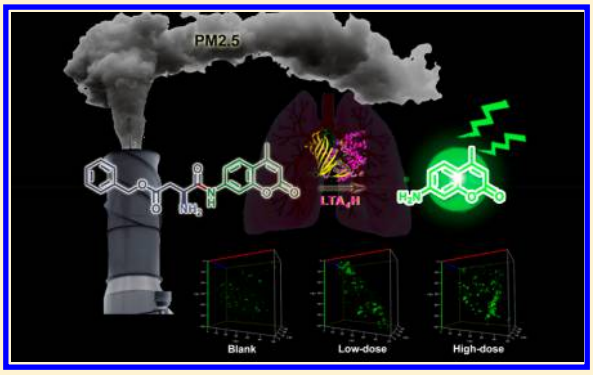

Regional haze pollution and increasing pollution levels have emerged in China and seriously threaten public health.[1,2] Studies of the 1952 London smog demonstrate that exposure to high concentrations of particulate matter can significantly increase the hospitalization and mortality rates associated with cardiopulmonary diseases.[3,4] Global epidemiological surveys show the direct relationship between the level of atmospheric particulates, including PM2.5, and the rate of pulmonary dysfunction or respiratory symptom diseases, such as pneumonia.[5−8] In general, pneumonia is a disease of the alveoli and respiratory bronchioles caused by pathogens, which induce local and systemic inflammatory responses in the patient.[9,10] Severe complications of pneumonia including meningitis, systemic sepsis, lung abscesses, brain damage, and hearing loss often occur.[11−14] The mortality rate of patients with pneumonia has remained high for the past decades. Thus, accurate diagnosis is essential for timely treatment of this disease. Clinically diagnosing pneumonia requires multiple techniques and clinical indices, including chest X-ray and CT imaging, culturing of blood and expectorated sputum samples, and evaluation of several suggestive clinical features.[15,16] Chest X-ray and CT imaging play crucial roles in the diagnosis but inflict considerable damages, such as cellular canceration, chromosomal aberration, and germ cell abnormality, which restrict their application.[17−19] Therefore, effective and rapid imaging approaches must be developed to accurately diagnose pneumonia.

Two-photon (TP) fluorescence imaging technology is a noninvasive method that uses highly sensitive and selective fluorescence probes.[20,21] In particular, the excitation at the near-infrared wavelength (690−950 nm) leads to increased tissue penetration depth, high temporal resolution, and reduced phototoxicity to tissues.[22] This imaging method can be used in vivo for study on cell metabolism and disease processes at the molecular level.[23] Therefore, TP fluorescence imaging using ideal fluorescent probes with high selectivity and sensitivity can be used to detect pneumonia biomarkers and effectively diagnose the disease in tissues of living systems.[24] LTA_4H (EC 3.3.2.6) is a key protein that mediates the degradation of peptides in host defense mechanism.[25,26] The expression level of LTA_4H significantly increases during inflammation and is related to the development and progression of inflammation.[27,28] Therefore, LTA_4H could be an effective biomarker for detecting pneumonia and estimating the effectiveness of the treatment and as a potential molecular target for pneumonia therapy.[19,29] However, existing detection kits for LTA_4H activity are only applied to the purified LTA_4H in vitro and cannot be used to obtain real physiological data in situ.[30] Moreover, the activity loss of LTA_4H caused by sample

Received: November 24, 2017
Accepted: April 23, 2018
Published: April 23, 2018

DOI: 10.1021/acs.analchem.7b04885
Anal. Chem. 2018, 90, 6020−6027

preparation may result in severe measurement error. Thus, a fluorescence probe with sensitive and selective response toward LTA_4H must be developed and used to accurately diagnose pneumonia by TP fluorescence imaging of the enzyme activity fluctuations in real time.

In this study, we propose a novel two-photon fluorescent probe (ASPC) for detection of LTA_4H activity in vivo. The structure of ASPC contained an amide bond linking the unnatural amino acid L-AspBzl as reaction site and 7-amino-4-methylcoumarin (AMC) as chromophore.[31] LTA_4H could specifically hydrolyze the amide bond between the carboxyl group of L-AspBzl and the amino group in AMC. Moreover, AMC was selected as the fluorescence reporting group because of its desirable photophysical properties, such as high fluorescent quantum yield, good photostability, and large Stokes shifts.[32] In ASPC, the reduction in the electron-cloud density of the nitrogen atom by the carbonyl group weakens the electron donor−acceptor interactions in the conjugated system of AMC, leading to decreased fluorescence quantum yield of AMC. After LTA_4H recognizes the substrate L-AspBzl in the active center and cleavages the amide bond, the fluorescence intensity of the probe recovers (Scheme 1). ASPC

Scheme 1. Schematic of Design and Mechanism of Fluorescent Probes for LTA_4H Activity

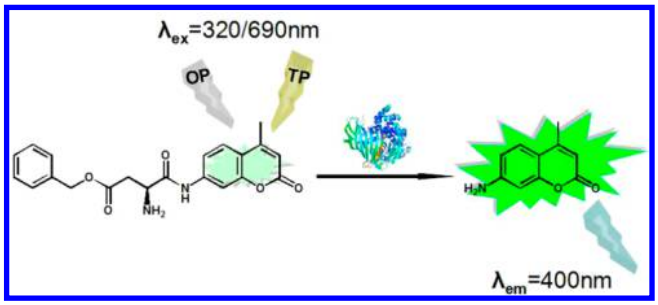

was used to measure the activity of LTA_4H for the first time and obtain the TP fluorescence images of LTA_4H in living cells and tissues. Based on the detected activity of LTA_4H in the lung tissues, mice exposed to PM2.5 were also diagnosed with pneumonia.

EXPERIMENTAL SECTION

Materials and Methods. All reagents were purchased commercially and used without further purification. All chemicals and solvents used were of analytical grades. Ultrapure water (18.2 MΩ cm^{-1}) was used throughout the analytical experiments. Boc-L-aspartic acid 4-benzyl ester (Boc-L-Asp (OBzl)−OH) was purchased from Aladdin, and 7-amino-4-methylcoumarin (AMC) was purchased from Ark Pharm, Inc.; lipopolysaccharide (LPS) and 3-(4,5-dimethylthiazol-2-yl)-2, 5-diphenyltetrazolium bromide (MTT) were purchased from Sigma. Ubenimex was from Energy Chemical. Silica gel (200−300 mesh) used for flash column chromatography was purchased from Qingdao Haiyang Chemical Co., Ltd. A549 human lung adenocarcinoma cell line and human hepatic stellate cells (LX-2) were purchased from Cell Bank of the Chinese Academy of Sciences (Shanghai, China). Recombinant human leukotriene A_4 hydrolase (LTA_4H) was purchased from Abcam. Aminopeptidases N (APN) and leucine aminopeptidases (LAP) were purchased from Cloud-Clone Corp., and methionine aminopeptidases (METAP) was purchased from Novoprotein. mouse interieukin-1β enzyme-linked immunosorbent assay (ELISA) kit was purchased from Sinobestbio (ShangHai, China).

^1H NMR and ^{13}C NMR spectra were determined by using Bruker NMR spectrometers at 400 and 100 MHz. The high-resolution mass spectra (HRMS) were measured with Bruker Maxis ultrahigh-resolution TOF MS system. The fluorescence spectra measurements were performed using an FLS-920 Edinburgh fluorescence spectrometer. Absorption spectra were measured with a TU-1900 UV−vis spectrophotometer (Beijing Purkinje General Instrument Co., Ltd.). Absorbance was measured with a microplate reader (RT 6000, Rayto, USA). Fluorescence imaging in cells and in vivo were performed with Zeiss LSM 880 NLO confocal laser scanning microscope. PM2.5 was collected from Jinan atmosphere by using an integrated intelligent air total suspended particulate sampler with a PM2.5 cutter (Laoying 2030, Laoshan Applicable Technology Institute, Qingdao, China).

Synthesis of ASPC. ASPC was synthesized according to the procedure in Supporting Information Scheme S1, and its structure characterization was described in the Supporting Information.

Specificity of ASPC toward LTA_4H. Fluorescence responses of ASPC (0.1 μM) reacted with different kinds of species for 90 min at 37 °C in a final volume of 200 μL of Tris-HCl (100 mM, pH 7.4) and NaCl (100 mM). Such as Zn^{2+} (50 mM), Ca^{2+} (50 mM), Mg^{2+} (50 mM), alanine (Ala, 1.0 mM), arginine (Arg, 1.0 mM), cysteine (Cys, 1.0 mM), glycine (Gly, 1.0 mM), lysine (Lys, 1.0 mM), glucose (50 mM), vitamin C (Vc, 1.0 mM), and LTA_4H (4 ng mL^{-1}). Cleavage of ASPC (0.1 μM) by other aminopeptidases such as APN, LAP, and METAP was also investigated.[33−35] The enzymes were tested in the following conditions: APN (5.0 μg mL^{-1}) in Tris-HCl buffer (100 mM, pH 7.5), LAP (5.0 μg mL^{-1}) in PBS buffer (50 mM, pH 7.4), and MAP (5.0 μg mL^{-1}) in Hepes buffer (50 mM, pH 7.4) and NaCl (100 mM). The reactions were performed in a final volume of 200 μL and incubated for 90 min at 37 °C. At the end of the reaction, fluorescence was measured on a FLS-920 Edinburgh fluorescence spectrometer (λ_{ex} = 320 nm; λ_{em} = 400 nm). Each experiment was repeated at least three times.

Kinetic Parameters of ASPC toward LTA_4H. Determination of the Michaelis constant (K_m) was performed in initial rate conditions. For this purpose, recombinant human LTA_4H (4 ng mL^{-1}) was added to increasing concentrations of ASPC in a final volume of 200 μL of Tris-HCl (100 mM, pH 7.4) and NaCl (100 mM) and incubated at 37 °C for 40 min. The substrate concentrations for K_m determination ranged from 0.05 to 50 μM. The AMC concentration and corresponding relative fluorescence unit was calculated by total hydrolysis of independent substrates at the same concentration. The average value was used for further calculations. Each experiment was repeated at least three times, and results are presented as mean ± SD. The K_m values were calculated using GraphPad Prism 6 software, and the K_{cat} was determined using the equation $K_{cat} = V_{max}/[E]$. Fluorescence was measured on a FLS-920 Edinburgh fluorescence spectrometer (λ_{ex} = 320 nm; λ_{em} = 400 nm).

Inhibitory Potency Measurements. To determine the in vitro inhibitory potencies or inhibitory constant (K_i) values of ubenimex toward LTA_4H, recombinant enzyme (4 ng mL^{-1}) was preincubated for 30 min at 37 °C in Tris-HCl (100 mM, pH 7.4) and NaCl (100 mM), with increasing concentrations of inhibitor (from 10^{-9} to 10^{-3} M final concentration). The

DOI: 10.1021/acs.analchem.7b04885
Anal. Chem. 2018, 90, 6020−6027

fluorescent substrates ASPC (10 μM) were added in a final volume of 200 μL and incubated at 37 °C for 40 min. The fluorescent values were measured on a FLS-920 Edinburgh fluorescence spectrometer (λ_{ex} = 320 nm; λ_{em} = 400 nm). Samples with 0% hydrolysis were obtained by adding the substrate to the buffer, and samples with 100% relative activity were prepared without the inhibitor. The percentage of cleavage was evaluated and compared with 100% relative activity, and the IC_{50} values were determined accordingly. The IC_{50} values were calculated using GraphPad Prism 6 software. The K_i values of the inhibitors (mean of at least three independent assays in duplicate) were calculated using the equation $K_i = IC_{50}/(1 + [S]/K_m)$, assuming their mode of binding to be competitive.

Cells Culture. A549 human lung adenocarcinoma cells and human hepatic cells (HL-7702) were respectively cultured in Roswell Park Memorial Institute (RPMI-1640) and Dulbecco's modified Eagle medium (DMEM) supplemented with 10% fetal bovine serum (FBS), 1% penicillin, and 1% streptomycin at 37 °C in a 5% CO_2/95% air incubator MCO-15AC (SANYO, Tokyo, Japan). Two days before imaging, the cells were detached and replanted on glass-bottomed dishes or 6-well dishes.

Cytotoxicity Assays. The cytotoxicity of ASPC toward A549 cell lines was measured by 3-(4,5-dimethylthiazol-2-yl)-2,5-diphenyltetrazolium bromide (MTT) assay. A549 cells were seeded in a 96-well plate at a concentration of 1×10^5 cells well^{-1} in 100 μL of RPMI-1640 medium with 10% fetal bovine serum, 1% penicillin, and 1% streptomycin and maintained at 37 °C in a 5% CO_2 incubator for 12 h. Then, cells were exposed to different concentrations of ASPC (0.01, 0.1, 1, 5, 10, and 20 μM) for 24 h. The cells were washed with 37 °C PBS, and MTT solution (5 mg mL^{-1}, 20 μL) was added to each well and continuously incubated for 4 h at 37 °C. After 4 h, MTT solution was removed and DMSO (150 μL) was added to each well to dissolve the dark blue formazan crystals. Absorbance was measured at 490 nm in a Triturus microplate reader. Cell viability was expressed as a percentage of MTT reduction with the untreated cells as 100%.

siRNA Transfection. LTA_4H protein expression in A549 was knocked out using LTA_4H-specific siRNA (sense, 5′-CAA AGG ACC UUA CAA UAG ATT-3′, antisense, 5′-UCU AUU GUA AGG UCC UUU GTT-3′; GenePharma, Shanghai, China). To verify transfection efficiency, we used FAM-siRNA (sense, 5′-UUC UCC GAA CGU GUC ACG UTT-3′; antisense, 5′-ACG UGA CAC GUU CGG AGA ATT-3′) as negative control. One day before transfection, A549 cells (4×10^5 total) were seeded in 6-well dishes by medium without antibiotics. For each transfection sample, siRNA:lipofectamine 2000 complexes were prepared as follows: siRNA (3 μL) and lipofectamine 2000 (5 μL) were diluted in 200 μL of Opti-MEM I, respectively. And then they were gently mixed before siRNA:lipofectamine 2000 complexes were added to each well. Finally, the cells were incubated at 37 °C for 48 h until they were ready to assay for gene knockdown.

Quantitative Real-Time PCR. RT-PCR was performed with the Linegene 9620 detection system using Power SYBR Green PCR master mix (Applied Biosystems). Total RNA was extracted using a UNlQ-10 Column total RNA Purification Kit (Sangon Biotech). All data were normalized to the level of the β-actin (sense, 5′-TCCCTGGAGAAGAGCTACG-3′; antisense, 5′-GTAGTTTCGTGGATGCCACA-3′) in the sample. Three independent technical replicates were performed for each reaction.

Western Blot. A549 cells grown in 6-well dishes were washed twice with cold PBS and lysed in 200 μL of RIPA lysis buffer containing protease inhibitors (1 mM PMSF). Lysate samples were incubated for 25 min at 4 °C. Samples were homogenized using cell scrapers and centrifuged at 12,000 rpm for 7 min at 4 °C. The supernatant was recovered, and protein concentration was determined by the Bradford assay. Then, lysate samples were added to SDS-PAGE loading buffer and heated for 5 min at 95 °C. After that, analysis by Western blotting were accomplished by Yuci Biotechnology Co.

OP and TP Fluorescence Imaging of HL-7702 Cells and A549 Cells. For the detection of endogenously produced LTA_4H, the cells were divided into three groups and treated with different conditions. (a) Blank cells: The cells were only incubated with ASPC (10 μM) in Tris-HCl (100 mM) at room temperature for 40 min. (b) LPS-treated cells: The cells were incubated with 10 μg mL^{-1} LPS in RPMI 1640 at 37 °C for 2 h. Then the cells were treated with ASPC (10 μM) in Tris-HCl (100 mM) at room remperature for 40 min. (c) LPS +ubenimex-treated cells: The cells were incubated with 10 μg mL^{-1} LPS in RPMI 1640 at 37 °C for 2 h. After 2 h, the cells were treated with ubenimex (1 μM) in Tris-HCl at room temperature for 40 min, and then cells were treated with ASPC (10 μM) for another 40 min. The cells were washed three times with Tris-HCl prior to the imaging. One-photon and two-photon fluorescent images were acquired on an LSM 880 NLO confocal laser scanning microscope with a water objective lens (20×). The excitation wavelengths were 405 and 690 nm, respectively.

TP Fluorescence Imaging and Flow Cytometry Imaging of A549 Cells after siRNA Transfection. The cells were divided into five groups and treated with different conditions. (a) Blank cells (blank group): A549 cells were pretreated with Tris-HCl (100 mM) for 2 h, and then incubated with ASPC (10 μM) for 40 min. (b) LPS cells (LPS group): A549 cells were pretreated with LPS (10 μg mL^{-1}) for 2 h and then incubated with ASPC (10 μM) for 40 min. (c) LPS+ubenimex cells: A549 cells were pretreated with LPS (10 μg mL^{-1}) for 2 h and treated with ubenimex (1 μM) for 40 min, and then cells were incubated with ASPC (10 μM) for 40 min. (d) siRNA cells (siRNA group): A549 cells pretreated with LTA_4H-specific siRNA were pretreated with Tris-HCl (100 mM) for 2 h and then incubated with ASPC (10 μM) for 40 min. (e) LPS+siRNA cells (siRNA LPS group): A549 cells treated with LTA_4H siRNA were pretreated with LPS (10 μg mL^{-1}) for 2 h and then incubated with ASPC (10 μM) for 40 min. Two-photon fluorescent images were acquired on an LSM 880 NLO confocal laser scanning microscope with a water objective lens (20×). The excitation wavelength was 690 nm.

Mice. All female KM mice and female BALB/c mice were purchased from Shandong University Laboratory Animal Center. All the animal experiments were carried out in accordance with the relevant laws and guidelines issued by the Ethical Committee of Shandong University.

LPS-Induced Abdominal Inflammation Model of Mice. All female KM mice (16−20 g) were divided into three groups and treated with different conditions. (A) Blank mice: the mice were pretreated with PBS for 4 h and then injected ASPC for 30 min. (B) LPS-induced mice: the mice were pretreated with LPS (2 mg mL^{-1}, 400 μL) for 4 h and injected ASPC for 30 min. (C) LPS+ubenimex-treated mice: the mice were pre-

DOI: 10.1021/acs.analchem.7b04885
Anal. Chem. 2018, 90, 6020−6027

treated with LPS for 4 h, then ubenimex was injected for 30 min, and then the mice were injected by ASPC for 30 min. Then, mice were anesthetized with 4% chloral hydrate (3 mL kg^{-1}) by intraperitoneal injection, and the hair and skin on the ventral surface of the abdomen was removed. Two-photon fluorescent images were acquired on an LSM 880 NLO confocal laser scanning microscope with a water objective lens (20×). The excitation wavelength was 690 nm (6 mW).

In Vivo Lung Inflammation Model of Mice. Six to eight week old female BALB/c mice were anesthetized with 4% chloral hydrate (3 mL kg^{-1}) by intraperitoneal injection. While anesthetized, the mice were located on a 45° plate and the mouse's tongue was pulled by tweezers. The mice were treated with LPS (167 μg mL^{-1}) through intranasal administration. After that, the mouse's nose was held immediately. After 20 s, the mice were released by the tongue and nose and made to wake up in the cage naturally. The mice were randomly divided into four groups: two groups of LPS-treated mice were injected with 20 μL of LPS (167 μg μL^{-1}) through intranasal route for 12 and 24 h; and the two other groups of blank mice were injected with the same amount of PBS.

In fluorescence imaging experiments, mice were injected with ASPC (200 μM, 50 μL) in the right lung after LPS administration (0, 12, and 24 h). The mice lungs were expose to a thoracotomy. Two-photon fluorescent images were acquired on an LSM 880 NLO confocal laser scanning microscope with an objective lens (10×). The excitation wavelength was 690 nm.

Measurement of Lung homogenate Interleukin-1β Levels. After the mice model was constructed successfully, the mice were killed by cervical dislocation. The lungs from the mice were excised and washed 3 times repeatedly with 100 mL of saline. Then, the lungs were abraded and lung homogenate was obtained. To each sample was added 1 mL of saline, and they centrifuged at 4 °C, 3000 rpm, and 10 min. The supernatant was collected. After that, we could measure the concentration of interleukin-1β (IL-1β) by using a standard ELISA kit. The IL-1β ELISA kit includes a set of calibration standards. The calibration standards are assayed at the same time as the samples and allowed the operator to produce a standard curve of optical density (O.D.) versus IL-1β concentration. The concentration of IL-1β in the sample is then determined by comparing the O.D. (450 nm) of the sample to the standard curve.

PM2.5 Model of Mice. PM2.5 was collected from Jinan atmosphere by using an integrated intelligent air total suspended particulate sampler with a PM2.5 cutter. PM2.5 was collected on glass fiber filters placed inside the sampler beforehand, and the flow rate was set to 120 L min^{-1} for 24 h. The filters were collected and washed with distilled water by using an ultrasonic cleaning machine. The residue of the filters was removed, and the particles were freeze-dried in vacuum. The obtained PM2.5 was stored at 4 °C in the dark. The suspensions were prepared before instillation.

Six to eight week old female BALB/c mice were randomly divided into three groups, which were injected with 20 μL of normal saline (control group), 20 μL of low-dose PM2.5 suspensions (7.5 mg mL^{-1} in normal saline), and 20 μL of high-dose PM2.5 suspensions (15 mg mL^{-1} in normal saline), respectively, through tracheal instillation for 3 days. After 24 h, we incubated mice with the ASPC and performed two-photon fluorescence imaging.

Statistical Analyses. The results are presented as the mean ± SEM. The statistical significance was evaluated using two-tailed Student's *t*-test: *, $P < 0.05$; **, $P < 0.01$; ***, $P < 0.001$.

RESULTS AND DISCUSSION

Chemical Synthesis of ASPC. Fluorescent probe ASPC could be readily synthesized in a yield of 25.6% under mild conditions (Scheme S1). The structure of ASPC was well characterized by ^{1}H NMR, ^{13}C NMR, and HRMS techniques (Figures S7–S9).

Photophysical Properties and Selectivity of ASPC. The spectral properties of the ASPC were investigated under physiological conditions (100 mM Tris buffer, pH 7.4) (Figure S1a–d). The ASPC displayed a distinct absorption maximum band at 320 nm and emitted a faint fluorescence at around 400 nm under excitation at 320 nm (Figure 1a). Upon the addition of LTA_4H, the fluorescence intensity at 400 nm increased, and the fluorescence quantum yield increased from 0.04 to 0.61. The probe exhibited a large Stokes shift of about 80 nm, thereby alleviating any efficiency loss attributed to self-absorption and reduced excitation interference. The fluorescence emission spectra of ASPC were also examined 120 min after adding LTA_4H. Figure 1b shows that the ASPC displays an 8-fold fluorescence enhancement at 400 nm after 120 min in the presence of LTA_4H. The TP properties of the ASPC were also investigated under the same physiological conditions. The ASPC is excited at 690 nm and emits at 400 nm. Upon treatment with LTA_4H, the TP fluorescence intensity increased dramatically at 400 nm and the two-photon cross-section of the ASPC is 25 GM.[36] All these data reveal that the ASPC can detect changes in LTA_4H activity.

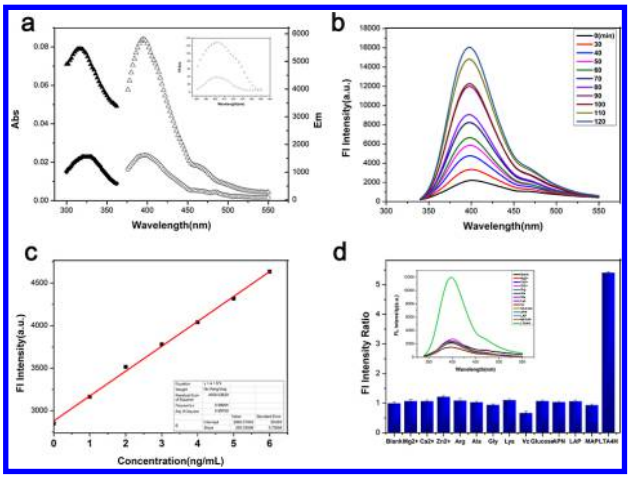

Figure 1. Photophysical properties and selectivity of ASPC. (a) One-photon excitation and emission spectra for ASPC (0.1 μM) before (●, ○) and after (▲, △) addition of LTA_4H (4 ng mL^{-1}). Inset: TP emission spectra for ASPC before (○) and after (△) addition of LTA_4H. (b) Fluorescence emission spectra scan of ASPC reacted with LTA_4H. (c) Linear relationship between fluorescence intensity of ASPC and LTA_4H concentrations (0–6.0 ng mL^{-1}). (d) Fluorescence responses of ASPC reacted with different kinds of species for 90 min (100 mM Tris buffer, 100 mM NaCl, pH = 7.4, 0.30% DMSO, v/v, 37 °C). Error bars represent standard deviation (n = 3).

We subsequently investigated the response of the ASPC toward different concentrations of LTA_4H. The probe was incubated with various concentrations of LTA_4H in Tris buffer at 37 °C for 1 h. Upon the addition of LTA_4H, the fluorescence

DOI: 10.1021/acs.analchem.7b04885
Anal. Chem. 2018, 90, 6020–6027

intensity at 400 nm was considerably enhanced (Figure 1c). A good linear relationship was obtained between the fluorescence intensity of the ASPC and the concentrations of LTA_4H (0−6.0 ng mL^{-1}), with a detection limit of 0.2183 ng mL^{-1} (R^2 > 0.99). Hence, the ASPC exhibited satisfactory response to the enzyme and can detect the activity of LTA_4H with excellent sensitivity under physiological conditions.

In addition, the kinetic parameters of ASPC toward LTA_4H were also investigated. Under the optimized condition, the calculated values of Michaelis constant K_m and K_{cat} were 21.18 ± 3.23 μM and 0.58 ± 0.04 S^{1-} (Figure S2b), respectively, indicating that ASPC binds to LTA_4H with excellent affinity. In order to prove that ASPC could be used to assess inhibitor potency, the K_i value of an aminopeptidase inhibitor—ubenimex—was determined using ASPC. Results showed that ubenimex inhibited the activity of LTA_4H with K_i = 58.5 ± 1.21 nM (Figure S2a), which is approximate with the previous report.[37] Therefore, we believe that ASPC is promising as a convenient tool for accurately screening specific depressors of LTA_4H.

To further evaluate the selectivity of the ASPC to LTA_4H, we examined various biologically relevant molecules, such as aminopeptidases (APN, METAP, and METAP), amino acids (glycine, alanine, cysteine, lysine, and arginine), metal ions (Zn^{2+}, Mg^{2+}, and Ca^{2+}), and glucose. The fluorescence intensity of ASPC did not evidently increase in the presence of the other relevant substances (Figure 1d). After coculture with LTA_4H under physiological conditions, the fluorescence intensity of the ASPC obviously increased. These results indicate that ASPC exhibits good selectivity for LTA_4H over other biologically relevant species. Thus, ASPC could be used to detect the activity of LTA_4H in complex biological systems.

To prove that ASPC can be applied in complex biological systems, we investigated the cytotoxicity of the probe toward cells through standard MTT assay. No obvious cytotoxicity was observed at concentrations up to 20 μM (Figure S1e). Additionally, the fluorescence photostability of ASPC in living cells was investigated (Figure S4). All these data demonstrate that ASPC exhibits low cytotoxicity and good photostability. Hence, ASPC can act as an excellent fluorescence probe in vivo.

Endogenous LTA_4H Imaging in Live Cells with ASPC. To assess the applicability of the ASPC as a two-photon fluorescent probe for imaging intracellular LTA_4H activity in biological systems, we tested the probe in living cells. The two-photon confocal fluorescence image of LTA_4H was applied to human hepatic cells (HL-7702). A cellular model of inflammation was successfully established by LPS stimulation, where inflammatory cytokines, such as LTA_4H, were overexpressed.[38,39] After treating two groups of HL-7702 cells with Tris-HCl (100 mM) (as control group) or LPS (10 μg mL^{-1}) for 2 h, the cells were incubated with ASPC (10 μM) at 37 °C for 40 min and washed with Tris-HCl to remove residual probes. The weak OP and TP fluorescence images were observed in blank cells (Figure 2). By contrast, the fluorescence intensity of the ASPC increased obviously upon the addition of LPS. This finding indicates the higher activity of LTA_4H in LPS-treated cells than that in blank cells. To confirm that the increase in the fluorescence intensity could be due to the high activity of LTA_4H, we added the inhibitor of LTA_4H into LPS-treated cells and observed changes in fluorescence. We selected ubenimex as the inhibitor of LTA_4H because it can competitively occupy the activity center of LTA_4H and inhibit the catalytic activity.[40,41] LPS+ubenimex-treated cells showed

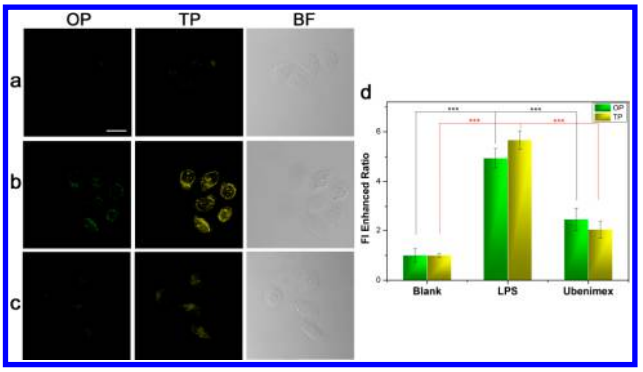

Figure 2. Fluorescence images of ASPC in human hepatic stellate cells (HL-7702). One-photon (OP) and two-photon (TP) fluorescence images of HL-7702 cells incubated with 10 μM ASPC for 40 min. (a) Blank cells. (b) LPS-treated cells. (c) LPS+ubenimex-treated cells. One-photon images were acquired using 405 nm excitation and 410−520 nm emission windows. TP imaging: λ_{ex} = 690 nm; λ_{em} = 380−520 nm. Scale bar = 200 μm. (d) Relative OP and TP fluorescence intensities of ASPC-labeled cells from images. Error bars represent standard deviation (n = 3). Statistical analysis performed with a two-tailed Student's t-test: ***, P < 0.001.

lower fluorescence intensity than LPS-treated cells (Figure 2g,h). Hence, the ASPC exhibits high sensitivity and selectivity to LTA_4H and can be applied for fluorescence imaging of enzyme activity in live cells.

To demonstrate the selective fluorescence response of the ASPC to intracellular LTA_4H, we performed *lta*$_4$*h* gene silencing in A549 cells by using small interfering RNA (siRNA).[42] The transfection results of FAM-labeled siRNA indicated an average transfection efficiency of approximately 92.6% (Figure S5). The efficiency of gene silencing was verified by Western blot (Figure 3g) and real-time PCR analyses (Figure S1f).[43,44] All these results suggest that the expression of LTA_4H was successfully suppressed in siRNA-treated cells. Compared with blank A549 cells without any stimulation, cells

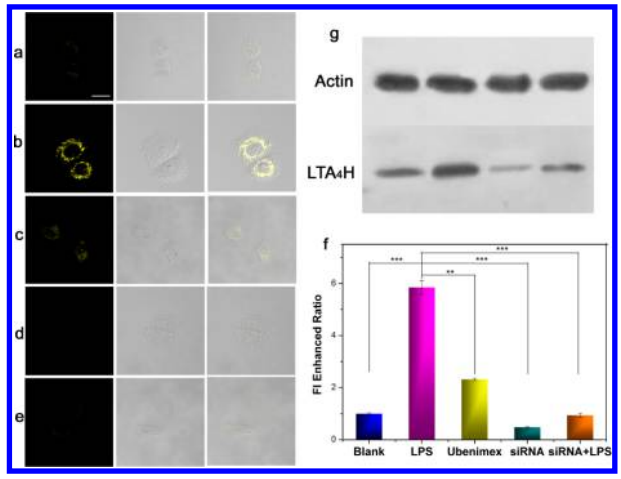

Figure 3. TP confocal images of LTA_4H in A549 cells. (a) Blank cells. (b) LPS cells. (c) LPS+ubenimex cells. (d) siRNA cells. (e) LPS +siRNA cells. TP imaging: λ_{ex} = 690 nm; λ_{em} = 380−520 nm. Scale bar = 200 μm. (f) Relative TP fluorescence intensities of ASPC-labeled cells from images. Error bars represent standard deviation (n = 3). Statistical analysis performed with a two-tailed Student's t-test: **, P < 0.01; ***, P < 0.001. (g) LTA_4H levels were analyzed with Western blot. From left to right, LTA_4H protein was extracted from blank cells, LPS cells, siRNA cells, and siRNA+LPS cells, respectively.

DOI: 10.1021/acs.analchem.7b04885
Anal. Chem. 2018, 90, 6020−6027

pretreated with LTA_4H siRNA showed a reduced fluorescence enhancement fold from 1 to 0.5 (Figure 3a,d). After stimulating with LPS for 2 h, the fluorescence enhancement decreased from 5.8-fold in LPS-treated cells to 0.9-fold in LPS+siRNA-treated cells (Figure 3b,e). Hence, ASPC can monitor the activity of endogenous LTA_4H in living cells with high sensitivity and excellent selectivity. Moreover, TPM fluorescence imaging using the ASPC as probe is a powerful method to effectively detect inflammation at the cellular level.

To investigate the applicability of ASPC to high-throughput screening, we used the ImageStreamX platform in analyzing the fluorescence intensity of ASPC in different cells. The capability of ASPC to detect LTA_4H in different cells was investigated, and the mean fluorescence intensity in thousands of cells was precisely calculated. LPS-pretreated A549 cells exhibited the strongest fluorescence intensity (the mean FI = 66706.96) compared with cells subjected to the other pretreatments (Figure 4). Hence, ASPC could be an imaging tool for high-efficiency, high-throughput monitoring of LTA_4H activity in vivo with high sensitivity.

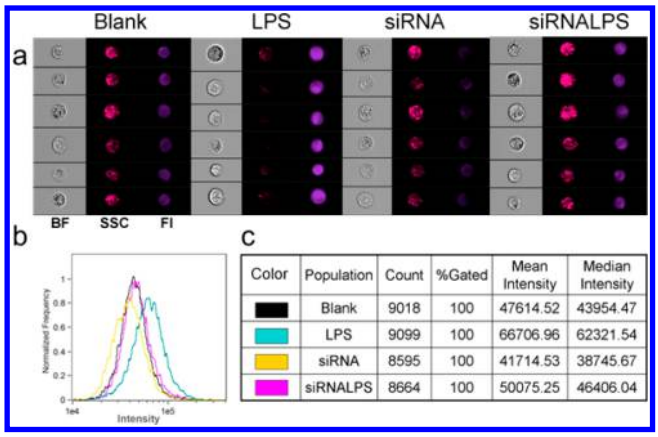

Figure 4. Determination of LTA_4H in A549 cells by imaging flow cytometry with four different treated conditions. (a) BF, bright field; SSC, fluorescence of side scatter; FI, fluorescence of ASPC. (b, c) Internalization score (>8000 cells).

In Vivo Fluorescence Imaging of LTA_4H in Mice by ASPC. The performance of ASPC as a fluorescent probe for animal bioimaging in vivo was further investigated. A mouse model of abdominal inflammation was constructed successfully by intraperitoneal injection of LPS into living mice.[45] After 4 h, the mice were injected with ASPC prior to TP imaging. Figure 5 shows that the fluorescence intensity in the abdominal tissues of inflamed mice (LPS-induced mice) is 4.2 times higher than that in healthy mice (blank mice without stimulus). After pretreatment with the inhibitor of LTA_4H-ubenimex, the fluorescence intensity in mice (LPS+ubenimex -treated mice) is only 2.1 times higher than that in healthy mice. This finding reveals that the LTA_4H protein in LPS-induced mice was overexpressed, leading to the strong fluorescence intensity of ASPC. Meanwhile, adding ubenimex to ASPC could inhibit the catalytic activity of LTA_4H and prevent fluorescence enhancement. Hence, ASPC shows high selectivity for detecting the activity of LTA_4H in mice.

Since LTA_4H in mice and human share highly identical protein sequences (http://www.ncbi.nlm.nih.gov/guide/proteins/), we used female mice as the live model. To verify the applicability of the ASPC for accurate diagnosis of

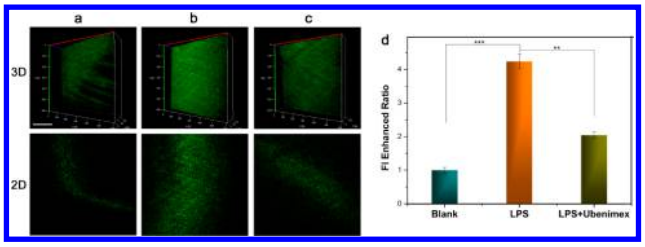

Figure 5. TP fluorescence imaging of LTA_4H in the mice model of abdominal inflammation. (a) Blank mice. (b) LPS-induced mice. (c) LPS+ubenimex-induced mice. (d) Fluorescence intensity enhanced ratios from images. TP imaging: λ_{ex} = 690 nm; λ_{em} = 380−520 nm. Scale bar = 200 μm. Error bars represent standard deviation (n = 4). Statistical analysis performed with a two-tailed Student's t-test: **, P < 0.01; ***, P < 0.001.

pneumonia, we performed two-photon fluorescence imaging with ASPC for detecting the activity of LTA_4H in LPS-induced mice with pneumonia.[29,46] Six to eight week old female BALB/c mice (16−18 g) were randomly divided into four groups: two groups of LPS-treated mice were injected with 20 μL of LPS (167 $\mu g\ \mu L^{-1}$) through intranasal route for 12 and 24 h; and the two other groups of blank mice were injected with the same amount of PBS. After injecting the ASPC for 30 min, two-photon fluorescence imaging of the lung tissues of mice was conducted. The fluorescence intensity in the lung tissues of LPS-treated mice is higher than that in blank mice (Figure 6). In addition, the fluorescence intensity increased by 4.6- and 5.3-fold under LPS stimulation for 12 and 24 h, respectively. This result indicates that the LPS-treated mice exhibit higher LTA_4H activity in the lung and might have pneumonia after LPS stimulation. IL-1β is one of the critical indicators of pneumonia.[47−49]

To confirm whether LPS-treated mice have pneumonia, we assessed the amount of IL-1β by using a commercial ELISA kit. After stimulation for 12 and 24 h, the concentrations of IL-1β are 2.9 and 3.6 times higher in LPS-treated mice than that in blank mice, respectively (Figure 6f). These data suggest that LPS-treated mice suffer from pneumonia, and their conditions continue to deteriorate over time. During this process, the expression level of LTA_4H in the lung tissues continually increased, resulting in an increased fluorescence signal of ASPC. Hence, LTA_4H can be used as an inflammatory biomarker for fluorescence imaging to accurately diagnose pneumonia.

Considering the successful establishment of a novel two-photon fluorescence imaging for accurately diagnosing pneumonia, we investigated whether haze particulates can cause pneumonia in mice.[7,8,50] A contaminated mouse model exposed to PM2.5 was built successfully. Six to eight week old female BALB/c mice (16−18 g) were randomly divided into three groups, which were injected with 20 μL of normal saline (control group), 20 μL of low-dose PM2.5 suspensions (7.5 mg mL^{-1} in normal saline), and 20 μL of high-dose PM2.5 suspensions (15 mg mL^{-1} in normal saline) through tracheal instillation for 3 days. After 24 h, we incubated mice with ASPC and performed two-photon fluorescence imaging. The fluorescence intensities in the lungs of mice that received PM2.5 suspensions are 1.6 (low-dose) and 2.9 times (high-dose) higher than that in the control group (Figure 7). This finding indicates the increased LTA_4H expression in the lungs of mice and the gradual deterioration of pneumonia with increasing particulate dosage. A commercial ELISA kit was adopted to measure the amount of IL-1β in the lung homogenates from

DOI: 10.1021/acs.analchem.7b04885
Anal. Chem. 2018, 90, 6020−6027

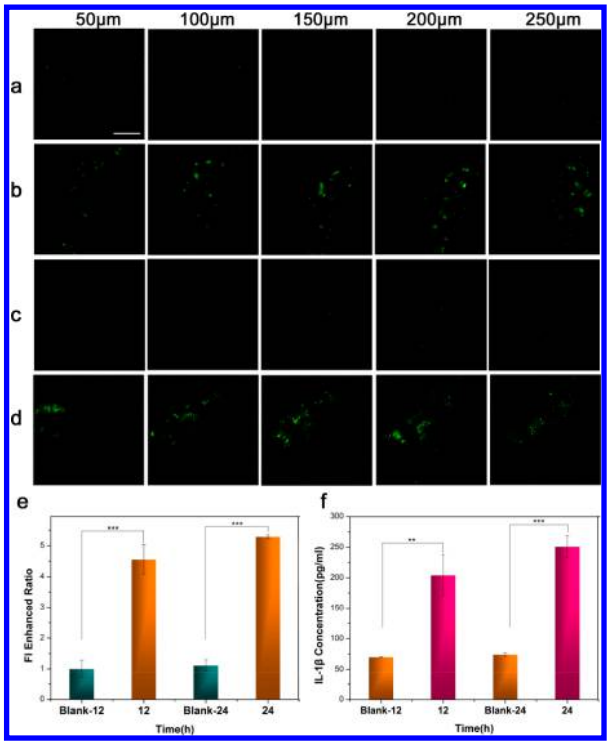

Figure 6. TP fluorescence imaging of LTA_4H in the mice model of lung inflammation with different times. Lungs of mice were incubated with ASPC (10 μM) for 30 min. (a, c) BALB/c mice injected with PBS (20 μL) for 12 and 24 h, respectively. (b, d) BALB/c mice injected with 20 μL of LPS (167 μg μL^{-1}) for 12 and 24 h, respectively. Labels from 50 to 250 μm indicate scanning depths of the lung tissue. (e) Fluorescence intensity enhanced ratios from images with different times. (f) Concentration of IL-1β measured at different times in lung homogenate of mice. Error bars represent standard deviation (n = 4). Statistical analysis performed with a two-tailed Student's t-test: **, $P < 0.01$; ***, $P < 0.001$. TP imaging: λ_{ex} = 690 nm; λ_{em} = 380−520 nm. Scale bar = 200 μm.

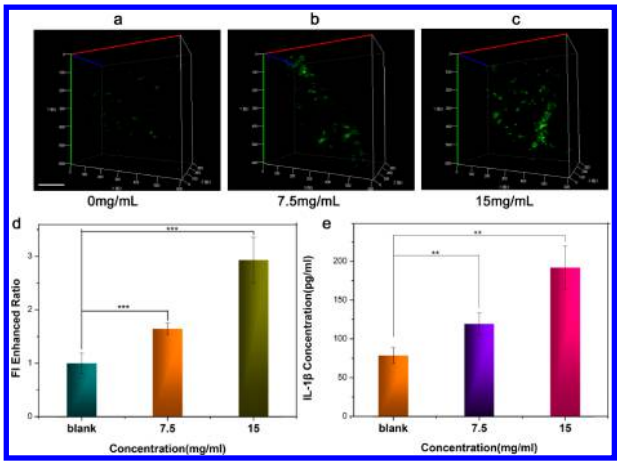

Figure 7. 3D volume-rendered TP imaging of LTA_4H in PM2.5 contaminated mice. (a) Blank group: mice injected with normal saline. (b) Mice injected with low-dose PM2.5 (7.5 mg mL^{-1}). (c) Mice injected with high-dose PM2.5 (15 mg mL^{-1}). (d) Fluorescence intensity enhanced ratios from images with different PM2.5 concentrations. (e) Concentration of IL-1β measured by different PM2.5 concentrations in lung homogenate of mice. TP imaging: λ_{ex} = 690 nm; λ_{em} = 380−520 nm. Scale bar = 200 μm. Error bars represent standard deviation (n = 4). Statistical analysis performed with a two-tailed Student's t-test: **, $P < 0.01$; ***, $P < 0.001$.

the mice. The amount of IL-1β in the homogenates increased with increasing dosage of PM2.5 (Figure 7e), consistent with the result of the two-photon fluorescence imaging. Hence, the contaminated mice that inhaled haze particulates (PM2.5) may suffer from pneumonia.

CONCLUSION

A novel two-photon fluorescence probe, namely, ASPC, was developed and used for highly sensitive and selective imaging of the inflammatory biomarker LTA_4H to rapidly and accurately diagnose pneumonia. The developed fluorescence probe is the first reported for specific detection of LTA_4H activity in vivo. ASPC possesses distinct advantages, including low cytotoxicity and deep tissue penetration depth, and can be used for rapid and real-time TP fluorescence imaging of LTA_4H in situ in cells and tissues. The probe was successfully applied for in situ visualization of LTA_4H activity in the lungs and for determining the gradual deterioration stage of pneumonia caused by increasing haze particulates dosage in the mouse model. With these outstanding advantages, the ASPC can be an indicator of pneumonia in vivo and can be used not only to diagnose pneumonia but also to estimate the effectiveness of treatment. The novel ASPC probe and imaging strategy could be a novel method for screening specific inhibitors of LTA_4H as potential drug candidates in the future.

ASSOCIATED CONTENT

Supporting Information

The Supporting Information is available free of charge on the ACS Publications website at DOI: 10.1021/acs.analchem.7b04885.

Organic synthesis, characterization, experimental details, and additional figures (PDF)

AUTHOR INFORMATION

Corresponding Authors

*(B.T.) E-mail: tangb@sdnu.edu.cn. Tel.: 86-531-86180010.
*(P.L.) E-mail: lip@sdnu.edu.cn. Tel.: 86-531-86180010.

ORCID

Bo Tang: 0000-0002-8712-7025

Author Contributions

†H.W. and K.X. contributed equally to this work.

Notes

The authors declare no competing financial interest.

ACKNOWLEDGMENTS

This work was supported by the 973 Program (Grant No. 2013CB933800), the National Natural Science Foundation of China (Grant Nos. 21405097, 21535004, and 21390411), the Project of Shandong Province Higher Educational Science and Technology Program (Grant No. J14LC04), and the Primary Research Plan in Shandong Province (Grant No. 2016GSF201205).

REFERENCES

(1) Huang, R. J.; Zhang, Y.; Bozzetti, C.; Ho, K. F.; Cao, J. J.; Han, Y.; Daellenbach, K. R.; Slowik, J. G.; Platt, S. M.; Canonaco, F.; Zotter, P.; Wolf, R.; Pieber, S. M.; Bruns, E. A.; Crippa, M.; Ciarelli, G.; Piazzalunga, A.; Schwikowski, M.; Abbaszade, G.; Schnelle-Kreis, J.; Zimmermann, R.; An, Z.; Szidat, S.; Baltensperger, U.; El Haddad, I.; Prevot, A. S. *Nature* **2014**, *514*, 218−222.
(2) Li, M.; Zhang, L. *Environ. Pollut.* **2014**, *189*, 85−86.

DOI: 10.1021/acs.analchem.7b04885
Anal. Chem. 2018, 90, 6020−6027

(3) Hunt, A.; Abraham, J. L.; Judson, B.; Berry, C. L. *Environ. Health Perspect* **2003**, *111*, 1209−1214.
(4) Bell, M. L.; Davis, D. L.; Fletcher, T. *Environ. Health Perspect.* **2004**, *112*, 6−8.
(5) Schwartz, J. *Environ. Res.* **1993**, *62*, 7−13.
(6) Meszaros, D.; Markos, J.; FitzGerald, D. G.; Walters, E. H.; Wood-Baker, R. *BMJ. Open Respir Res.* **2015**, *2*, e000063.
(7) Jing, Y.; Zhang, H.; Cai, Z.; Zhao, Y.; Wu, Y.; Zheng, X.; Liu, Y.; Qin, Y.; Gu, M.; Jin, J. *Evid Based Complement Alternat Med.* **2017**, *2017*, 1575793.
(8) Wang, H.; Song, L.; Ju, W.; Wang, X.; Dong, L.; Zhang, Y.; Ya, P.; Yang, C.; Li, F. *Sci. Rep.* **2017**, *7*, 44256.
(9) Fernandez-Serrano, S.; Dorca, J.; Coromines, M.; Carratala, J.; Gudiol, F.; Manresa, F. *Clin. Diagn. Lab. Immunol.* **2003**, *10*, 813−820.
(10) Knapp, S.; Leemans, J. C.; Florquin, S.; Branger, J.; Maris, N. A.; Pater, J.; van Rooijen, N.; van der Poll, T. *Am. J. Respir. Crit. Care Med.* **2003**, *167*, 171−179.
(11) Chen, Y.; Deng, W.; Wang, S. M.; Mo, Q. M.; Jia, H.; Wang, Q.; Li, S. G.; Li, X.; Yao, B. D.; Liu, C. J.; Zhan, Y. Q.; Ji, C.; Lopez, A. L.; Wang, X. Y. *PLoS One* **2011**, *6*, e27333.
(12) Pugin, J.; Suter, P. M. *Intensive Care Med.* **1992**, *18*, 6−10.
(13) Kuhajda, I.; Zarogoulidis, K.; Tsirgogianni, K.; Tsavlis, D.; Kioumis, I.; Kosmidis, C.; Tsakiridis, K.; Mpakas, A.; Zarogoulidis, P.; Zissimopoulos, A.; Baloukas, D.; Kuhajda, D. *Ann. Transl. Med.* **2015**, *3* (13), 183.
(14) Yang, S.; Stepien, D.; Hanseman, D.; Robinson, B.; Goodman, M. D.; Pritts, T. A.; Caldwell, C. C.; Remick, D. G.; Lentsch, A. B. *Crit. Care Med.* **2014**, *42*, 2092−2100.
(15) Self, W. H.; Courtney, D. M.; McNaughton, C. D.; Wunderink, R. G.; Kline, J. *A. Am. J. Emerg Med.* **2013**, *31*, 401−5.
(16) Fang, G.-D.; Fine, M.; Orloff, J.; Arisumi, D.; Yu, V. L.; Kapoor, W.; Grayston, J. T.; Wang, S. P.; Kohler, R.; Muder, R. R.; Yee, Y. C.; Rihs, J. D.; Vickers, R. M. *Medicine (Philadelphia, PA, U. S.)* **1990**, *69*, 307−316.
(17) Gohagan, J. K.; Marcus, P. M.; Fagerstrom, R. M.; Pinsky, P. F.; Kramer, B. S.; Prorok, P. C.; Ascher, S.; Bailey, W.; Brewer, B.; Church, T.; Engelhard, D.; Ford, M.; Fouad, M.; Freedman, M.; Gelmann, E.; Gierada, D.; Hocking, W.; Inampudi, S.; Irons, B.; Johnson, C. C.; Jones, A.; Kucera, G.; Kvale, P.; Lappe, K.; Manor, W.; Moore, A.; Nath, H.; Neff, S.; Oken, M.; Plunkett, M.; Price, H.; Reding, D.; Riley, T.; Schwartz, M.; Spizarny, D.; Yoffie, R.; Zylak, C. *Lung Cancer* **2005**, *47*, 9−15.
(18) Abbruzzese, J. L.; Abbruzzese, M. C.; Lenzi, R.; Hess, K. R.; Raber, M. N. *J. Clin. Oncol.* **1995**, *13*, 2094−2103.
(19) Brock, T. G.; Lee, Y. J.; Maydanski, E.; Marburger, T. L.; Luo, M.; Paine, R. R.; Peters-Golden, M. *Am. J. Physiol-Lung C* **2005**, *289*, L224−L232.
(20) Zhou, L.; Zhang, X.; Wang, Q.; Lv, Y.; Mao, G.; Luo, A.; Wu, Y.; Wu, Y.; Zhang, J.; Tan, W. *J. Am. Chem. Soc.* **2014**, *136*, 9838−9841.
(21) Zhang, W.; Liu, W.; Li, P.; Kang, J.; Wang, J.; Wang, H.; Tang, B. *Chem. Commun. (Cambridge, U. K.)* **2015**, *51*, 10150−10153.
(22) Zhang, W.; Li, P.; Yang, F.; Hu, X.; Sun, C.; Zhang, W.; Chen, D.; Tang, B. *J. Am. Chem. Soc.* **2013**, *135*, 14956−14959.
(23) Zhang, W.; Wang, X.; Li, P.; Huang, F.; Wang, H.; Zhang, W.; Tang, B. *Chem. Commun. (Cambridge, U. K.)* **2015**, *51*, 9710−9713.
(24) Yuan, L.; Wang, L.; Agrawalla, B. K.; Park, S. J.; Zhu, H.; Sivaraman, B.; Peng, J.; Xu, Q. H.; Chang, Y. T. *J. Am. Chem. Soc.* **2015**, *137*, 5930−5938.
(25) Rudberg, P. C.; Tholander, F.; Andberg, M.; Thunnissen, M. M.; Haeggstrom, J. Z. *J. Biol. Chem.* **2004**, *279*, 27376−27382.
(26) Haeggstrom, J. Z.; Kull, F.; Rudberg, P. C.; Tholander, F.; Thunnissen, M. M. *Prostaglandins Other Lipid Mediators* **2002**, *68*−*69*, 495−510.
(27) Snelgrove, R. J.; Jackson, P. L.; Hardison, M. T.; Noerager, B. D.; Kinloch, A.; Gaggar, A.; Shastry, S.; Rowe, S. M.; Shim, Y. M.; Hussell, T.; Blalock, J. E. *Science* **2010**, *330*, 90−94.
(28) Thunnissen, M. M.; Nordlund, P.; Haeggstrom, J. Z. *Nat. Struct. Biol.* **2001**, *8*, 131−135.
(29) Akthar, S.; Patel, D. F.; Beale, R. C.; Peiro, T.; Xu, X.; Gaggar, A.; Jackson, P. L.; Blalock, J. E.; Lloyd, C. M.; Snelgrove, R. J. *Nat. Commun.* **2015**, *6*, 8423.
(30) Poras, H.; Duquesnoy, S.; Fournie-Zaluski, M. C.; Ratinaud-Giraud, C.; Roques, B. P.; Ouimet, T. *Anal. Biochem.* **2013**, *441*, 152−161.
(31) Byzia, A.; Haeggstrom, J. Z.; Salvesen, G. S.; Drag, M. *Amino Acids* **2014**, *46*, 1313−1320.
(32) Poreba, M.; Drag, M. *Curr. Med. Chem.* **2010**, *17*, 3968−3995.
(33) Chen, L.; Sun, W.; Li, J.; Liu, Z.; Ma, Z.; Zhang, W.; Du, L.; Xu, W.; Fang, H.; Li, M. *Org. Biomol. Chem.* **2013**, *11*, 378−382.
(34) He, X.; Li, L.; Fang, Y.; Shi, W.; Li, X.; Ma, H. *Chem. Sci.* **2017**, *8*, 3479−3483. Van de Bittner, G. C.; Bertozzi, C. R.; Chang, C. J. *J. Am. Chem. Soc.* **2013**, *135*, 1783−1795.
(35) Olaleye, O.; Raghunand, T. R.; Bhat, S.; He, J.; Tyagi, S.; Lamichhane, G.; Gu, P.; Zhou, J.; Zhang, Y.; Grosset, J.; Bishai, W. R.; Liu, J. O. *Chem. Biol.* **2010**, *17*, 86−97.
(36) Fisher, J. A.; Salzberg, B. M.; Yodh, A. G. *J. Neurosci. Methods* **2005**, *148*, 94−102.
(37) Thunnissen, M. M.; Andersson, B.; Samuelsson, B.; Wong, C. H.; Haeggstrom, J. Z. *FASEB J.* **2002**, *16*, 1648−1650.
(38) Rummel, C.; Inoue, W.; Poole, S.; Luheshi, G. N. *Mol. Psychiatry* **2010**, *15*, 523−534.
(39) Penning, T. D.; Chandrakumar, N. S.; Chen, B. B.; Chen, H. Y.; Desai, B. N.; Djuric, S. W.; Docter, S. H.; Gasiecki, A. F.; Haack, R. A.; Miyashiro, J. M.; Russell, M. A.; Yu, S. S.; Corley, D. G.; Durley, R. C.; Kilpatrick, B. F.; Parnas, B. L.; Askonas, L. J.; Gierse, J. K.; Harding, E. I.; Highkin, M. K.; Kachur, J. F.; Kim, S. H.; Krivi, G. G.; Villani-Price, D.; Pyla, E. Y.; Smith, W. G.; Ghoreishi-Haack, N. S. *J. Med. Chem.* **2000**, *43*, 721−735.
(40) Chen, X.; Li, N.; Wang, S.; Wu, N.; Hong, J.; Jiao, X.; Krasna, M. J.; Beer, D. G.; Yang, C. S. *J. Natl. Cancer Inst* **2003**, *95*, 1053−1061.
(41) Benner, J.; Daniel, H.; Spanier, B. *PLoS One* **2011**, *6*, e25624.
(42) Li, J.; Yu, J.; Zhao, J.; Wang, J.; Zheng, S.; Lin, S.; Chen, L.; Yang, M.; Jia, S.; Zhang, X.; Chen, P. R. *Nat. Chem.* **2014**, *6*, 352−361.
(43) Li, J. J.; Chu, Y.; Lee, B. Y.; Xie, X. S. *Nucleic Acids Res.* **2008**, *36*, e36.
(44) Lieschke, G. J.; Currie, P. D. *Nat. Rev. Genet.* **2007**, *8*, 353−367.
(45) Li, P.; Liu, L.; Xiao, H.; Zhang, W.; Wang, L.; Tang, B. *J. Am. Chem. Soc.* **2016**, *138*, 2893−2896.
(46) Yin, Q.; Fang, S.; Park, J.; Crews, A. L.; Parikh, I.; Adler, K. B. *Am. J. Respir. Cell Mol. Biol.* **2016**, *55*, 617−622.
(47) Conway Morris, A.; Kefala, K.; Wilkinson, T. S.; Moncayo-Nieto, O. L.; Dhaliwal, K.; Farrell, L.; Walsh, T. S.; Mackenzie, S. J.; Swann, D. G.; Andrews, P. J.; Anderson, N.; Govan, J. R.; Laurenson, I. F.; Reid, H.; Davidson, D. J.; Haslett, C.; Sallenave, J. M.; Simpson, A. *Thorax* **2010**, *65*, 201−207.
(48) Kolb, M.; Margetts, P. J.; Anthony, D. C.; Pitossi, F.; Gauldie, J. *J. Clin. Invest.* **2001**, *107*, 1529−1536.
(49) Lieberman, D.; Livnat, S.; Schlaeffer, F.; Porath, A.; Horowitz, S.; Levy, R. *Infection* **1997**, *25*, 90−94.
(50) Riva, D. R.; Magalhaes, C. B.; Lopes, A. A.; Lancas, T.; Mauad, T.; Malm, O.; Valenca, S. S.; Saldiva, P. H.; Faffe, D. S.; Zin, W. A. *Inhalation Toxicol.* **2011**, *23*, 257−267.

DOI: 10.1021/acs.analchem.7b04885
Anal. Chem. 2018, 90, 6020−6027